

# Effect of annealing temperatures on the morphology, optical and electrical properties of TiO<sub>2</sub> thin films synthesized by the sol–gel method and deposited on Al/TiO<sub>2</sub>/SiO<sub>2</sub>/p-Si

A. K. M. Muaz<sup>1,2</sup> · U. Hashim<sup>1,3</sup> · Fatimah Ibrahim<sup>2</sup> · K. L. Thong<sup>2</sup> · Mas S. Mohktar<sup>2</sup> · Wei-Wen Liu<sup>1</sup>

Received: 14 January 2015 / Accepted: 25 March 2015 / Published online: 3 April 2015  
© Springer-Verlag Berlin Heidelberg 2015

**Abstract** Fabrication and characterization of titanium dioxide (TiO<sub>2</sub>) thin film on Al/TiO<sub>2</sub>/SiO<sub>2</sub>/p-Si MIS structure for the study of morphology, optical and electrical properties were reported. A transparent and high crystallinity of TiO<sub>2</sub> thin films were prepared at room temperature (~25 °C) by sol–gel route. TiO<sub>2</sub> sol suspension were prepared at molar ratio of TTIP:EtOH:AA = 2:15:1 using titanium tetra-isopropoxide (TTIP) and a mixture of absolute ethanol (EtOH) and acetic acid (AA) which used as a precursor and catalyst for the peptization, respectively. The TiO<sub>2</sub> thin films were deposited on a thermally grown SiO<sub>2</sub> layer of p-type silicon (100) substrates and were thermally treated at different annealing temperatures of 300, 500, 700 and 900 °C. For study of optical properties, the TiO<sub>2</sub> thin films were deposited on a glass slides substrate and were annealed from 200 to 700 °C. The XRD results show that the presence of an amorphous TiO<sub>2</sub> phases were transformed into the polycrystalline (anatase or rutile) with good crystallinity after treated at higher annealing temperatures. Besides, the surface roughness of TiO<sub>2</sub> thin films increased with increasing annealing temperatures. In addition, the resistivity of the thin films decreased from 2.5751E+8 to 6.714E+7 Ω cm with the increasing temperatures.

Moreover, the optical absorbance of TiO<sub>2</sub> thin films exhibited high UV–visible light absorption with band gap energy shifted to the higher wavelength (low energy photons). The band gap energy ( $E_g$ ) of the films decreased from 3.79 to 3.16 eV and from 3.95 to 3.75 eV significantly for direct band allowed and indirect band allowed, respectively, with the increasing annealing temperatures.

## 1 Introduction

There are a large number of efforts have been carried out to find an alternative oxide with higher dielectric constant ( $k$ ) such as Al<sub>2</sub>O<sub>3</sub>, ZrO<sub>2</sub>, HfO<sub>2</sub>, Ta<sub>2</sub>O<sub>5</sub>, La<sub>2</sub>O<sub>2</sub>, Gd<sub>2</sub>O<sub>2</sub> and TiO<sub>2</sub> that are allowed to enhance gate capacitance and thus negate the effect of the associated leakage. Among these high- $k$  dielectric materials, titanium dioxide (TiO<sub>2</sub>) exhibits as the ideal candidate to replace the conventional oxide material of silicon dioxide (SiO<sub>2</sub>). It is because SiO<sub>2</sub> has become vulnerable to direct tunnelling (gate leakage) at a low dimensional which resulted indirectly drastic increases in the leakage current (Paily et al. 2002). Therefore, the design of nanostructures of TiO<sub>2</sub> thin films has attracted great attention around the world due to its unique electrical properties because it possess a credible alternative dielectric due to its higher dielectric constant and higher breakdown strength as compared to SiO<sub>2</sub> (Campbell et al. 1997). Thus, TiO<sub>2</sub> thin films have been widely used as a gate dielectric layer in metal oxide semiconductor (MOS) (Gou and Ma 1998). Besides, TiO<sub>2</sub> thin films is an n-type semiconductor with excellent optical properties such as wide energy band gap of 3.1 eV and high refractive index of 2.6 (Gugliemi et al. 1992).

There are a lot of application of TiO<sub>2</sub> such as gas sensors (Paul et al. 2012), dye-sensitized solar cells (Enache-Pommer et al. 2007), optical coatings (Tachibana et al. 2007),

✉ U. Hashim  
uda@unimap.edu.my

Wei-Wen Liu  
wwliu@unimap.edu.my

<sup>1</sup> Nanostructure Lab-on-chip Research Group, Institute of Nano Electronic Engineering, Universiti Malaysia Perlis, 01000 Kangar, Perlis, Malaysia  
<sup>2</sup> Departments of Biomedical Engineering, University of Malaya, 50603 Kuala Lumpur, Malaysia  
<sup>3</sup> School of Microelectronic Engineering, Universiti Malaysia Perlis, Pauh Putra Campus, 02600 Arau, Perlis, Malaysia

photo-catalysts (De Anda Reyes et al. 2012), biomedical fields (Jing-Xiao et al. 2003) and anti-microbial materials (Yaşa et al. 2012) because of non-toxic and good stability of  $\text{TiO}_2$  in various environments (Mathews et al. 2009a, b).  $\text{TiO}_2$  thin films can be prepared using several methods including radio frequency (RF) magnetron sputtering (Lijian et al. 1993; Turkevych et al. 2008), metal–organic chemical vapor deposition (Horprathum et al. 2012), spray pyrolysis (Oja et al. 2006), e-beam evaporation (Lottiaux et al. 1989), and sol–gel process (Brinker and Harrington 1981). However, among the methods mentioned above, the sol–gel method has a number of benefits than the other methods such as low reaction temperature, low cost production and simple steps are required, to synthesize a thin and homogeneity of film over a large area of substrates (Foo et al. 2011, 2012a, b, c, 2013, 2014). It is known that the physical properties of  $\text{TiO}_2$  material is highly dependent on the method of deposition and annealing temperature which influences the transformation of polycrystalline  $\text{TiO}_2$  thin films from amorphous to anatase and followed by rutile phase (Mathews et al. 2009a, b). In the present work,  $\text{TiO}_2$  thin films were prepared on a glass and *p*-type (100) orientation silicon substrates by using the cost effective sol–gel technique. To the best of our knowledge, this is considered the first report of the investigation on the effect of annealing temperatures on the  $\text{TiO}_2$  thin film deposited on the  $\text{Al}/\text{TiO}_2/\text{SiO}_2/\text{p-Si}$  from the perspective of crystalline structure, surface morphology, optical and electrical properties. Another significance of our work is the  $\text{Al}/\text{TiO}_2/\text{SiO}_2/\text{p-Si}$  structure shows smaller band gap energy which is very suitable for solar cell application.

## 2 Experimentation

### 2.1 Starting material

The high-*k*  $\text{TiO}_2$  thin films were deposited on a *p*-type <100> oriented silicon substrate which used as a starting material with the resistivity of 1–10  $\Omega$  cm and dimensions of 2.5 cm  $\times$  2.5 cm. Prior to the oxidation in high-temperature, the *p*-Si substrates were chemically cleaned using RCA-1, RCA-2 and Buffered Oxide Etchant (BOE) to remove any residual contamination matter (dirt, scum, silicon dust, etc.) and native oxide layers from the surface of the silicon wafers. The oxidation layer was deposited on the wafer substrate to reduce the parasitic device capacitance and indirectly enhance the performance of the final device. After that, the substrate surface was blown with  $\text{N}_2$  gas for drying purpose using the nitrogen spray gun. In order to perform the optical measurement, soda lime glass slides were used as a substrates to deposit the films. Prior to the deposition, the glass substrates were cleaned by rinsed

into deionized water and then immersed in Decon 90 in an ultrasonic bath for 2 h. The cleaned glass slides were dried in nitrogen ambient.

### 2.2 Thin films preparation

In sol–gel precipitation technique, nano-structure pure  $\text{TiO}_2$  thin films were prepared using titanium tetra-isopropoxide ( $\text{Ti}\{\text{OCH}(\text{CH}_3)_2\}_4$ ) with a purity of 97 %, acetic acid ( $\text{CH}_3\text{COOH}$ ) with a purity of 99.5 % and ethanol ( $M = 46.07 \text{ g mol}^{-1}$ ) with a purity of 99.8 % without any further purification. In order to obtain a stable sol solution, the proportion of  $\text{Ti}(\text{OC}_3\text{H}_7)_4$ ,  $\text{C}_2\text{H}_6\text{O}$  and  $\text{C}_2\text{H}_4\text{O}_2$  must be controlled to avoid the  $\text{TiO}_2$  films from crack upon annealing. The procedures for the preparation of  $\text{TiO}_2$  thin film was started with the dissolution of 8 mL of titanium tetra-isopropoxide into a 60 mL of ethanol to form a mixture which was magnetic stirred for 1 h. In final step, 4 mL of acetic acid were slowly dropped into the mixture and the final solution was subjected to the magnetic stirred for another 1 h. The composition of the obtained gel was TTIP:EtOH:AA with a ratio of 2:15:1. The mixture has a low condensation rate which enhanced the possibility of obtaining a stable and clear sol gel by spin coating process. The resultant homogeneous solutions were aged for 2 days in a stable environment before dispersed on the substrate surface.

### 2.3 Thin film deposition

To form double gate layers, firstly a  $\text{SiO}_2$  dielectric layer with thickness of 3000 Å was grown on the *p*-Si substrates by wet oxidation at 1000 °C for 1 h and then, following by the deposition of  $\text{TiO}_2$  thin film. Prior to the  $\text{TiO}_2$  thin films deposition, both of the glass slides and *p*-Si substrates were cleaned thoroughly using acetone and rinsed using isopropanol in ultrasonic bath. Then, they were heated at 100 °C for 15 min, and finally cooled naturally to room temperature. The  $\text{TiO}_2$  thin film were deposited on glass slides and *p*-Si substrates using spin coating technique which spun at 3500 rev./min for 30 s under suction. After the deposition, the  $\text{TiO}_2$  thin films were pre-heated at 80 °C for 30 min to evaporate the solvent and remove the organic residual. At least 5 successive deposition were done to form the required film thickness. For  $\text{TiO}_2/\text{p-Si}$ , the samples were inserted into the muffle furnace for annealing for 1 h at different annealing temperatures of 300, 500, 700 and 900 °C. For  $\text{TiO}_2/\text{glass slides}$ , the samples were annealed from 200 to 700 °C for an hour as well.

### 2.4 Thin film characterization

X-ray diffraction (XRD) (model D2 PHASER) was performed to determine the crystalline phase and to estimate

the crystallite size of the particles which annealed at various annealing temperatures. The XRD patterns were recorded by step scanning in the range of  $20\text{--}60^\circ$  with a step of  $0.02^\circ$  a measuring time of 5 s/step. All peaks measured by XRD analysis were identified by comparing with those of JCPDS data. A high-resolution atomic force microscopy (AFM) (model SPA-400) was performed to study the surface morphology which induced by thermal annealing under 2D imaging and projection of  $800 \times 800$  nm. The absorbance and transmittance of  $\text{TiO}_2$  thin films which coated on glass slide were examined at normal incident by using a UV–visible spectrometer (UV–VIS) (PerkinElmer model Lambda 35). The electrical resistivity of  $\text{TiO}_2$  thin films was measured at room temperature using the two-point probe technique coupled with sources meter (model Keithley 2400), interfaced by a Lab view Leios TMXpert simulator and voltage supply ranging from zero to +2 V was used. Electrical measurements were performed to investigate the electrical properties of the  $\text{TiO}_2$  thin films. In order to perform the electrical measurement, the Al/ $\text{TiO}_2$ / $\text{SiO}_2$ /p-Si metal insulator semiconductor (MIS) structure was developed by metalizing with aluminium (Al) on the silicon substrate thin films using a thermal evaporator (PVD) vacuum coater (model AUTO 306). To obtain a thickness of 300 nm of the deposited Al, current of 50 mA for 15 min, deposition rate of 5.3 nm/s and vacuum background pressure rate of  $50 \mu\text{Torr}$  were chosen. Figure 1 shows the overall experimental process in this research.

### 3 Result and discussions

#### 3.1 Morphological properties

Figure 2 illustrates the X-ray diffraction (XRD) pattern of  $\text{TiO}_2$  thin films. It clearly shows that the absence of spurious diffractions is good in agreement with the finding reported by Mulayam et al. (2010) which indicates that the high crystallinity of  $\text{TiO}_2$  thin film were formed. In Fig. 2, anatase phase, rutile phase and silicon substrate are denoted as A, R and Si, respectively. It was found that amorphous and polycrystalline phases were formed in the prepared  $\text{TiO}_2$  thin films. In Fig. 2a, the XRD diagrams of as-deposited (un-annealing sample) thin films shows that amorphous phase was formed only which is correlated with the work as reported by Kabasakaloglu et al. (2003). On the other hand, the diffraction patterns of samples annealed at 300 and 500 °C show the presence of diffraction peaks at (101), (004) and (200) planes, are assigned to the tetragonal anatase  $\text{TiO}_2$  lattice, as agreed with the JCPDS card no. 21-1272 (anatase  $\text{TiO}_2$ ). The increase of annealing temperatures from 300 to 500 °C increased the intensity of diffraction peaks, suggesting that the crystallinity of anatase

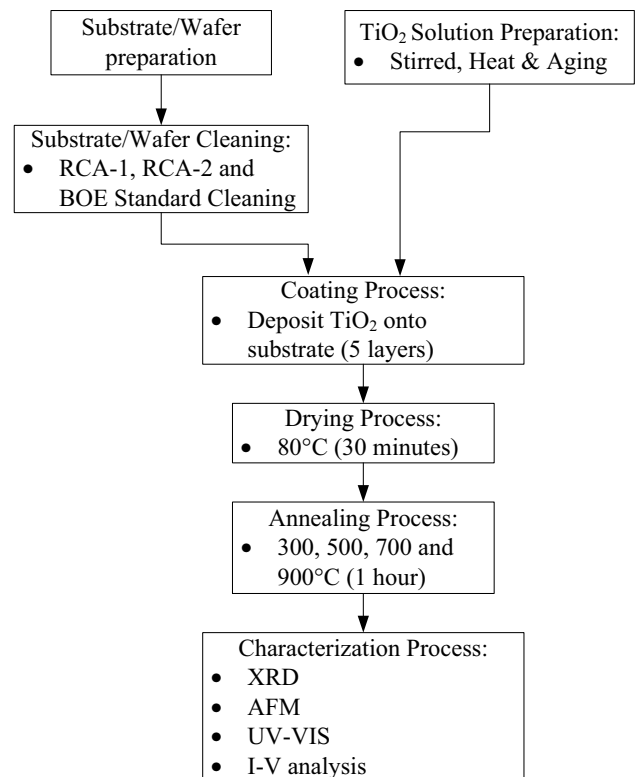


**Fig. 1** Flow chart of the preparation of nano- $\text{TiO}_2$  powders using a sol-gel technique

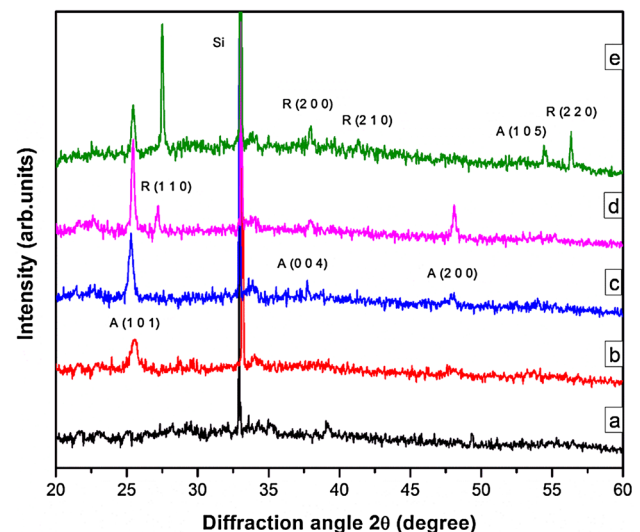


**Fig. 2** XRD pattern of  $\text{TiO}_2$  thin films **a** as-deposited (un-annealed sample), annealed at **b** 300, **c** 500, **d** 700 and **e** 900 °C, respectively

phase was increased, which is in agreement with the finding demonstrated by Hasan et al. (2008).

When  $\text{TiO}_2$  thin films were annealed at 700 °C, rutile and anatase phases were appeared at (110) and (101),

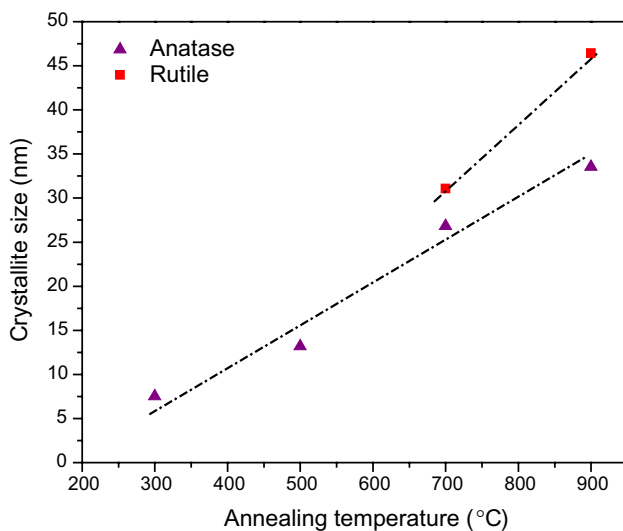


**Fig. 3** The increase of crystallite sizes of anatase and rutile phases at annealing temperatures of 300, 500, 700 and 900 °C

respectively. The diffraction peaks at  $33.5^\circ$  are assigned to the silicon substrate. It is noticeable that the amount of rutile phase (JCPDS card no 21-1276) increased with increasing annealing temperature from 700 to 900 °C. At 900 °C, the anatase phase disappeared and replaced by rutile phase, indicating that a complete transformation from the anatase phase to rutile phase has occurred which is in agreement with the work done by Jin Kim et al. (2002) that the anatase-to-rutile phase formation occurred at 1000 °C. The average crystallite sizes of the samples were estimated by considering the Debye–Scherrer’s equation as expressed below:

$$\text{Crystallite size, } D = 0.9\lambda / (\beta_{hkl} \cdot \cos \theta_{hkl}) \quad (1)$$

where  $D$  is diameter of crystalline,  $\lambda$  is the X-ray wavelength of Cu K $\alpha$  radiation,  $\beta_{hkl}$  is broadening of the  $hkl$  diffraction peak width at half height of the maximum intensity (FWHM) in radians and  $\theta_{hkl}$  is the diffraction angle (Bragg’s angle) in degrees. Figure 3 shows that an increase in annealing temperatures produces bigger crystallite size. For instance, when the annealing temperature increased from 300 to 900 °C, the crystallite size of the anatase phase increased from 7.53 to 46.43 nm for an annealing time of 1 h. The crystallite size of rutile phase also increased with the increasing annealing temperatures from 700 to 900 °C. For TiO<sub>2</sub> thin films containing anatase and rutile phase only, the percentage of mass fraction ( $X_A$ ) for anatase phase in the solution was calculated using the relative intensity of maximum peak of anatase phase (101) and a maximum peak of rutile phase (110). The  $X_A$  is expressed using the following equation (Spurr and Myers 1957);

$$\text{Mass fraction, } X_A = [1 + 1.265 \cdot I_R / I_A]^{-1} \quad (2)$$

**Table 1** Crystallite size (nm) and percentage of mass fraction ( $X_A$ ) for anatase and rutile phases in various annealing temperatures

Annealing temperature (°C)	Crystallite size (nm)		Mass fraction, $X_A$ (%)
	Anatase (1 0 1)	Rutile (1 1 0)	
As-deposited	–	–	–
300	7.53	–	100.00
500	13.19	–	100.00
700	26.83	31.08	64.17
900	33.54	46.43	29.53

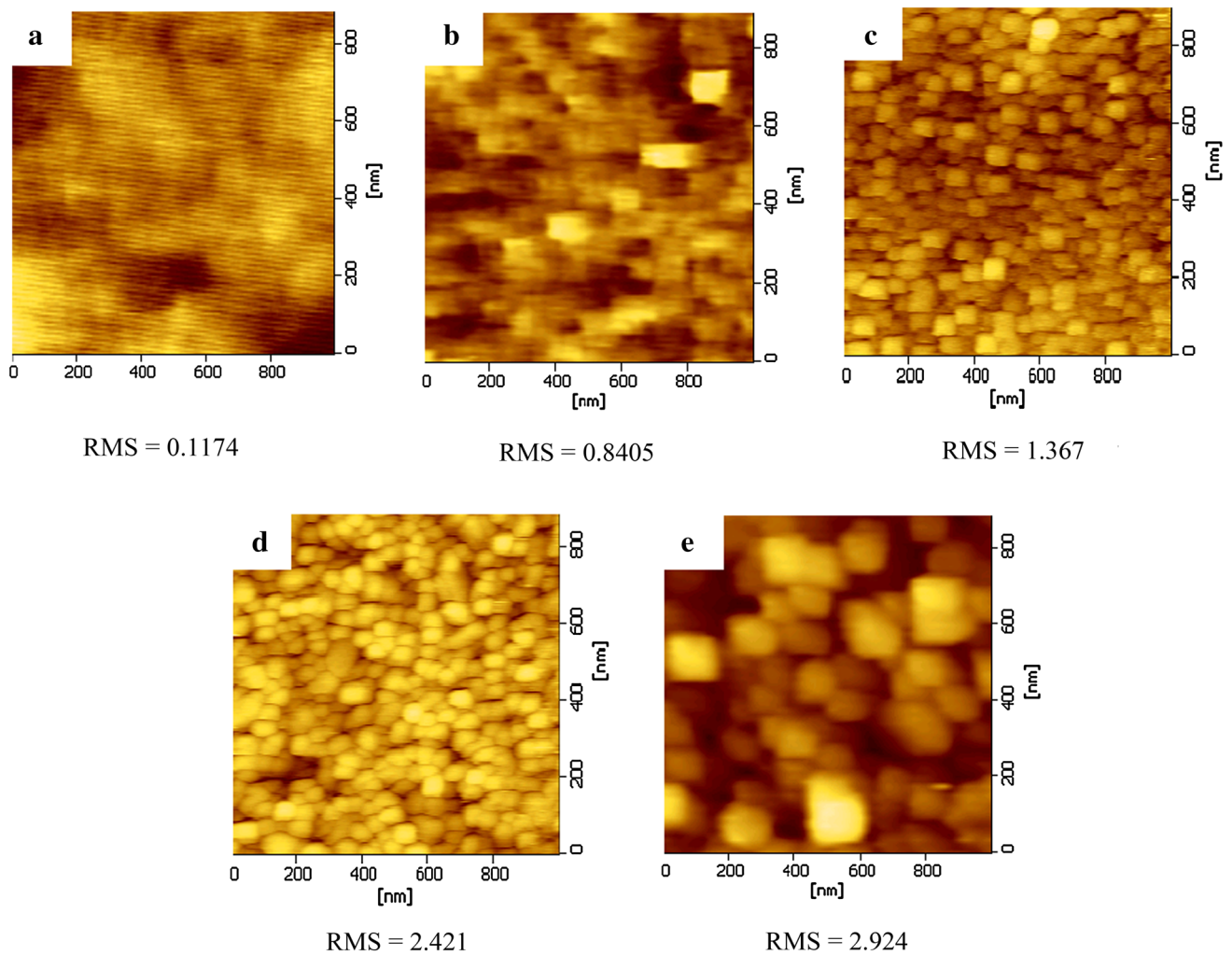
where  $X_A$  referred as a contents of anatase phase in the solutions,  $I_A$  is the intensity of the maximum anatase phase peak,  $I_R$  is the intensity of maximum rutile phase peak and 1.265 is the scattering coefficient (Zhu et al. 2007). In Table 1, it is observed that the  $X_A$  of anatase phase was 64.17 % and it decreased to 29.53 % as the annealing temperature increased from 700 to 900 °C, respectively. Rutile-anatase (mixed-phase photocatalysts) phase compositions of nanoparticles TiO<sub>2</sub> have been reported to exhibit enhanced photoactivity relative to single phase titania (Addamo et al. 2004; Ohno et al. 2001). It is considered widely that this is the result of improved charge carrier separation, possibly through the trapping of electrons in rutile and consequence reduction in electron–hole recombination (Ohno et al. 2003).

Figure 4 shows the surface morphologies of as-deposited TiO<sub>2</sub> thin films annealed at different temperatures of 300, 500, 700, 900 °C. In Fig. 4a, the AFM images show that smooth surface, compact, bulky, not uniform and column-like structure were observed for the TiO<sub>2</sub> thin films surface. Besides, AFM images also indicate that the changes of surface morphology and roughness of TiO<sub>2</sub> thin films were highly dependent on the annealing temperatures.

According to Wei et al. (2003), the key to improve the TiO<sub>2</sub> photocatalytic efficiency was to control the distribution and nanoparticle size of TiO<sub>2</sub> thin films. The calculated root mean square roughness (RMS) values were presented in Fig. 4. The results show that less than 1 nm of RMS was found for the as-deposited and annealed thin film at 300 and 500 °C. It increases with increasing annealing temperatures which suggesting that the regular grains shapes were formed in the TiO<sub>2</sub> thin films. Figure 4b is the surface morphologies image of TiO<sub>2</sub> thin films annealed at 300 °C. Some column-like crystal grains of 24.57 nm in diameter were seen in Fig. 4b. Our experiments are in agreement with the work done by Ya-Qi et al. (2003) that the annealed temperatures influenced the morphology of TiO<sub>2</sub> thin film and therefore, the anatase phase was formed at 300 °C.

When the annealing temperatures was increased to the 500 °C, the sample exhibited a preferred orientation of regular grains shaped, which suggesting the growth of the





**Fig. 4** 2-D AFM images of TiO<sub>2</sub> thin film **a** as-deposited, annealed at **b** 300 °C, **c** 500 °C, **d** 700 °C and **e** 900 °C, respectively. The scan area is 800 nm

crystalline structure of TiO<sub>2</sub>. It is noticeable that the RMS increased with increasing annealing temperatures from 700 to 900 °C (Fig. 4d, e), indicating that the grains sizes increased with increasing annealing temperatures. This shows that higher annealing temperatures resulted in the agglomeration of small grains to form larger grains. Consequently, anatase phase was transformed into rutile phase with increasing annealing temperatures (Richards 2002) as correlated with the work done by Mathews et al. (2009a, b) that the dramatic change of topography and crystallization of TiO<sub>2</sub> thin films were due to the increasing of thermal annealing temperatures. The AFM results are in good agreement with XRD analysis, which shows that the crystalline structures were formed at high annealing temperature.

The TiO<sub>2</sub> thin film thickness and surface roughness as a function of annealing temperatures is shown in Fig. 5.

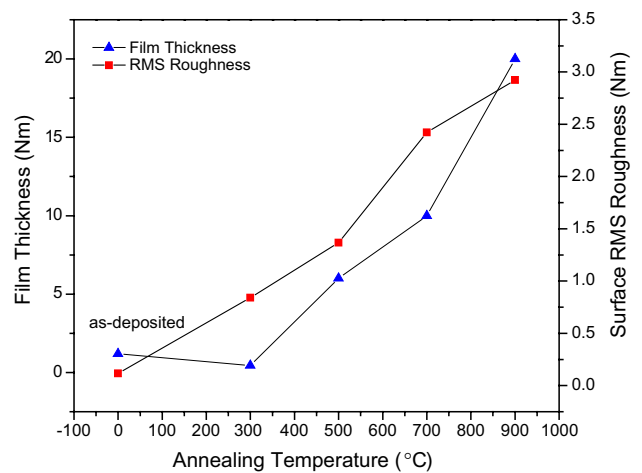


**Fig. 5** The increase of film thickness and surface roughness with the increase annealing temperatures

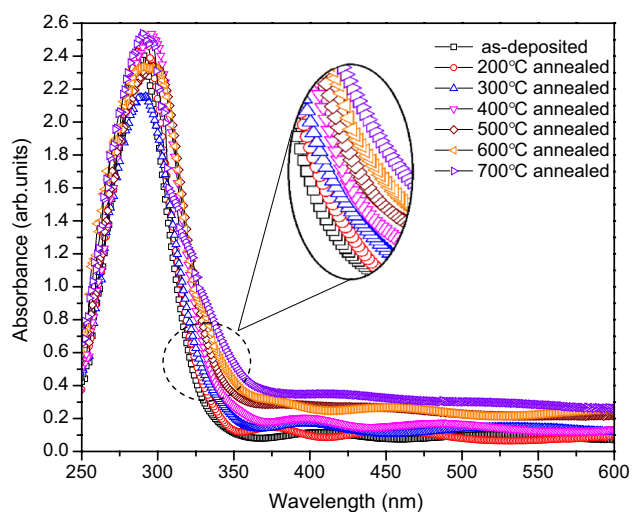


**Fig. 6** UV-Vis absorption spectra of as-deposited and annealed TiO<sub>2</sub> nanoparticles thin film at 200, 300, 400, 500, 600 and 700 °C

As expected, the film thickness and surface roughness significantly increased from 0.45 to 20 nm and from 0.841 to 2.924 nm, respectively, for the annealing temperatures range of 300–900 °C. The increase in thickness and roughness at the higher temperature probably was due to the growth of small grains sizes to larger and domed grains sizes. It also can be attributed to enhancement of nucleation and coalescence of grains (Dubal et al. 2011). This work is in agreement with the finding reported by Al-Obaidi and Yousif (2013) that surface roughness of the TiO<sub>2</sub> thin film increases with film thickness, annealing time and annealing temperatures.

### 3.2 Optical absorption and band gap

Figure 6 shows the UV–Visible light absorption spectra of prepared TiO<sub>2</sub> thin films which annealed at various temperatures under ambient conditions by scanning from 250 to 600 nm. The spectra reveals that an increases of annealing temperatures, the absorption edge is shifted to higher wavelength (low energy photons). The band gap energy ( $E_g$ ) of TiO<sub>2</sub> thin films were calculated according to the following equation (Zachariah et al. 2008):

$$\text{Band gap energy, } E_g = \frac{hc}{\lambda_{int}} \quad (3)$$

where  $h$  is Planck's constant,  $c$  is the speed of light and  $\lambda_{int}$ , the wavelength (nm) corresponding to the intersection of extension of linear parts of the spectrum y-axis and x-axis. The TiO<sub>2</sub> thin films exhibited a dramatically increase in absorption in excess of 250 nm (Fig. 6). Low absorption was seen in the visible region of 400–600 nm, which corresponds to the properties of TiO<sub>2</sub> thin films. In this region,

tailing of the absorbance was observed (Mayabadi et al. 2014). The energy gap of TiO<sub>2</sub> thin films and the absorption coefficient ( $\alpha$ ) were evaluated using an optical transmittance spectrum. From the measured transmittance ( $T$ ) given in Fig. 9, the optical absorption coefficient can be determined using the following relations (Subramaniam et al. 2009):

$$\text{Absorption coefficient, } \alpha = \frac{1}{d} \ln \left( \frac{1}{T} \right) \quad (4)$$

where  $d$  is the thickness of the films (from Fig. 5) and  $T$  is its transmittance values. It is known that TiO<sub>2</sub> has direct and indirect band gaps (Janitabar-Darzi et al. 2009). To evaluate the optical energy band gap of the TiO<sub>2</sub> thin films, Tauc plot model is applied in the region where the highest percentage of absorption appeared in the optical absorption spectra in Fig. 6. The relationship between the absorption coefficient ( $\alpha$ ) and the incident photon energy ( $h\nu$ ) is expressed as follows (Tauc et al. 1966):

$$\text{Tauc equation, } \alpha = \frac{K(h\nu - E_g)^n}{h\nu} \quad (5)$$

where  $K$  is constant depending on the transition probability,  $h\nu$  is photon energy,  $E_g$  is the optical band gap between the valence band and the conduction band and  $n$  is the power, which characterizes the type of electronic transition, either directly or indirectly during the absorption process. Specifically,  $n$  refers to is, 2, and 3 for direct allowed, indirect allowed, direct forbidden and indirectly forbidden transitions, respectively. The nature of the optical absorption transition can be determined by plotting a graph of  $(\alpha h\nu)^{1/2}$  as the function of the incident photon energy ( $h\nu$ ). The optical band gap  $E_g$  values are defined by extrapolation values of the absorption coefficient  $\alpha$  to a zero ( $(\alpha h\nu)^{1/2} = 0$ ). In Fig. 7, the energy gap for as-deposited and annealed TiO<sub>2</sub> thin films were found to decrease with increasing annealing temperatures in the range of 3.79 to 3.16 eV for direct allowed and from 3.95 to 3.75 eV for indirect allowed as listed in Table 2. The results show that the band gap energy of annealed TiO<sub>2</sub> thin films was smaller than the value of the as-deposited TiO<sub>2</sub> thin films, which can be attributed to the effect of increases of grain sizes with increasing annealing temperatures (Justicia et al. 2002). An increase of the grain sizes has weakened the quantum size effects and thus, lead to the decreased in the band gap energy and caused a gradually shift of the absorption edge towards a longer wavelength (Fig. 6) (red shift) (Kumar et al. 2012). Figure 8 shows the variations of the  $E_g$  for direct and indirect allowed as a function of film thickness. It can be seen that the band gap energy decreased with the increasing grain sizes and thickness of TiO<sub>2</sub> thin films due to the increases annealing temperatures as summarized in Table 2. This suggests that the grain sizes increased linearly with thickness

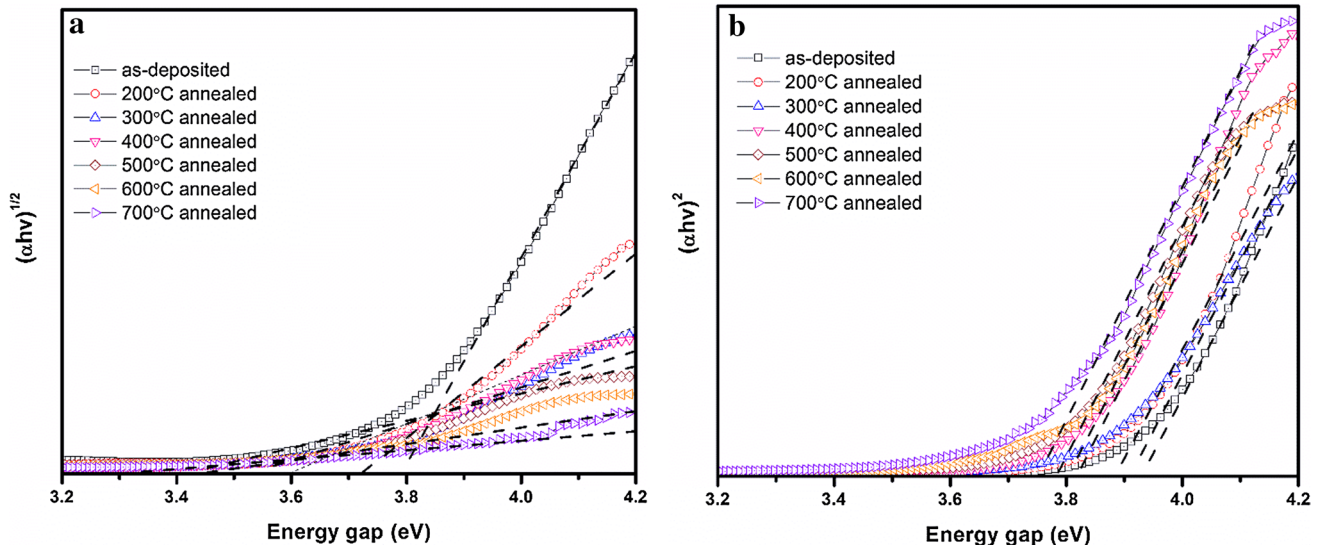


**Fig. 7** Tauc plot of  $(\alpha hv)^{1/2}$  vs.  $(hv)$  of the as-deposited and annealed  $\text{TiO}_2$  nanoparticles thin films **a** direct band gap and **b** indirect band gap

**Table 2** Determination of band gap energy of as-deposited and annealed  $\text{TiO}_2$  thin films

Sample (°C)	Absorption edge (nm)	Band gap energy ( $E_g$ )	
		Direct (eV)	Indirect (eV)
As-deposited	327	3.79	3.95
200	332	3.73	3.91
300	348	3.56	3.87
400	355	3.49	3.84
500	374	3.31	3.80
600	385	3.22	3.78
700	392	3.16	3.75

of  $\text{TiO}_2$  thin films (Tayade et al. 2007; Çörekçi et al. 2011). When the values of band gap decreased, densely packed crystalline structures of the films were formed (Kumar et al. 2012). The values of the band gap energy can support the XRD results in which large grain sizes are correlated with small band gap energy (46.43 nm, 3.16 eV) however, small grain sizes are correlated with large band gap energy (7.53 nm, 3.79 eV).

The transmittance of as-deposited and annealed thin films were recorded from 300 to 600 nm. In order to prevent the influence of the absorption edge on the substrate surface, the glass slides was used as the substrates in this

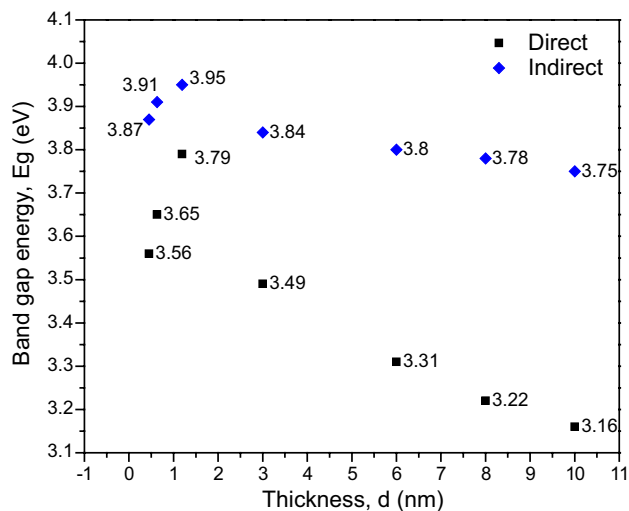


**Fig. 8** Plot of band gap energy of  $\text{TiO}_2$  films with different thickness

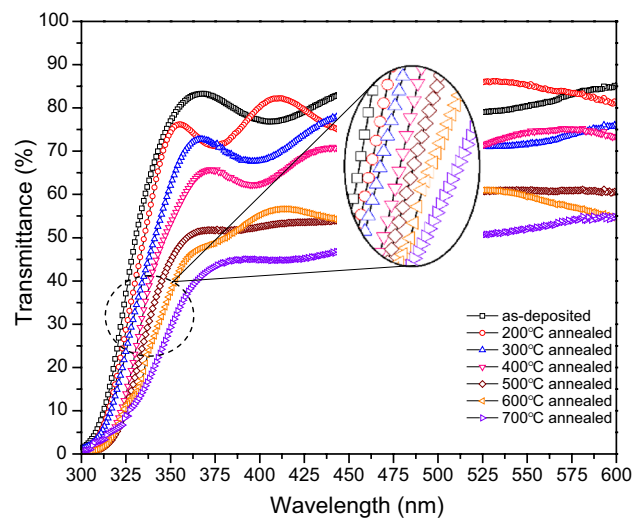


**Fig. 9** Transmittance spectrum of the  $\text{TiO}_2$  thin films coatings of as-deposited and annealed at different annealing temperatures

measurement. As shown in Fig. 9, a gradual increase in transmittance is observed with an increase of wavelength from 450 to 600 nm. The average transmittance of as-deposited and annealed films at 200, 300 and 400 °C show high transparencies of 85, 80, 75 and 70 %, respectively, in the visible region. The relatively high transmittance of the TiO<sub>2</sub> thin film indicates good homogeneity and low surface roughness (Hosseini et al. 2013). Focusing attention is paid to the transmittance spectrum where the transmittance began to fall-off rapidly at a wavelength about 340 nm for all TiO<sub>2</sub> thin films and approached zero at approximately 310 nm. The decreases of transmittance was due to the absorption of light had caused the excited electron to immigrate from the valence band (occupied band) to the conduction band (unoccupied band) of TiO<sub>2</sub> nanoparticles. It is noticeable that a slight reduces of transmittance values with the increasing annealing temperatures was observed. The TiO<sub>2</sub> thin films that annealed above 500 °C reveals significantly reduced in transmittance as compared to those for the film treated at 200 °C within the visible light region, indicates that the films became translucent after annealed at higher temperatures. At a temperature of 600 °C, the percentage of transmittance decreased about 45 % at the wavelength of 380 nm which corresponds to the band gap energy of TiO<sub>2</sub> (anatase). The decreases of transmittance for the films prepared at higher temperatures can be attributed to the annihilation of porous surfaces resulting from the increases of grain sizes, phase transformation from nanocrystalline anatase to rutile phase and diffusion of light scattering in the TiO<sub>2</sub> thin films (Habibi et al. 2010; Choi et al. 2010).

### 3.3 Electrical Properties

In order to measure the electrical resistivity and conductivity of the produced TiO<sub>2</sub> thin films, the current–voltage (I–V) measurements were performed using the circular Al dots as the metal contacts which applied to the surface of the TiO<sub>2</sub> thin films coated on silicon substrates. The measured current (I) was the current passing through the TiO<sub>2</sub> thin films, while the measured voltage (V) was the voltage that charge the capacitor. The results show that the value of current flow was extremely small as seen in Fig. 10. The measured electrical resistivity decreased with the increasing annealing temperatures. Figure 11 shows the effect of annealing temperatures on the resistivity ( $\rho$ ) and conductivity ( $\sigma$ ) for as-deposited and annealed thin films. The resistivity is expressed by the following equation:

$$\text{Resistivity, } \rho = \left(\frac{V}{I}\right) \left(\frac{A}{L}\right) \quad (6)$$

where  $V$  is the applied voltage,  $I$  is the current,  $A$  is the area of the film and  $L$  is the length of the electrode between two dots of the film. When the annealing temperatures

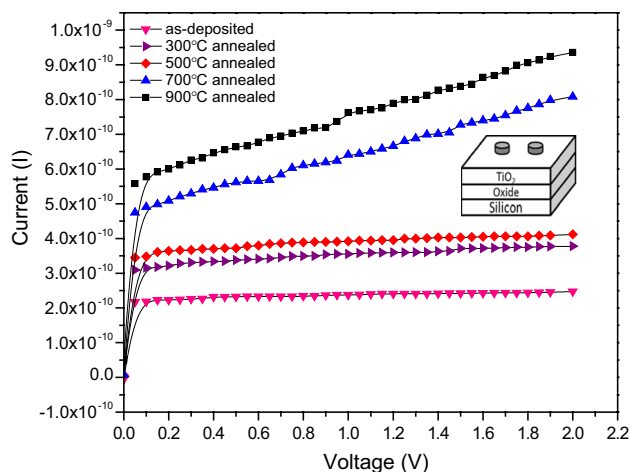


**Fig. 10** I–V characteristics for as-deposited and annealed TiO<sub>2</sub> thin films. The image inset shows the device structure

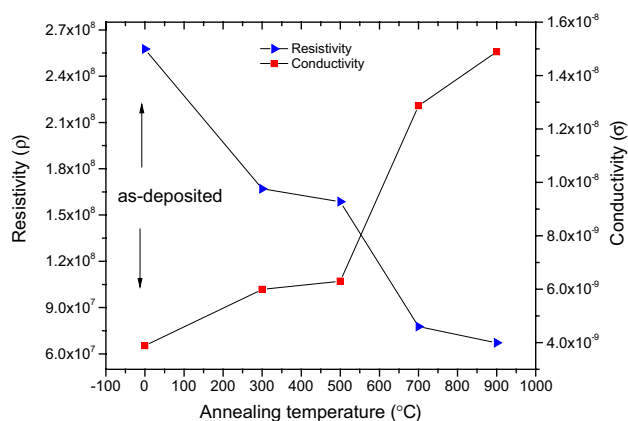


**Fig. 11** Resistivity and conductivity of as-deposited and annealed TiO<sub>2</sub> thin films

was increased, the resistivity decreased considerably and reached its minimum value of  $6.714\text{E}+7 \text{ } \Omega \text{ cm}$  for a TiO<sub>2</sub> thin films annealed at 900 °C. The decreases in resistivity over the annealing temperatures can be explained as follows: at a higher annealing temperature, the volume of the grains size became larger and increased the surface contact between the grains. Consequently, it improved the movement of electrons from one particle to the neighbouring particles and thus, decreased the size or thickness of grain boundaries and resistivity (Mathews et al. 2009a, b; Ahmad et al. 2010). Furthermore, the annealing treatment also produces better physical attachment which improves the electronic contacts between all the particles of the thin films (Ahmad et al. 2010). Since the TiO<sub>2</sub> is an n-type semiconductor materials, the existing concentration of Ti<sup>4+</sup> in TiO<sub>2</sub> films forms a donor level between the band gap of TiO<sub>2</sub> which reduced the recombination rate of photo-generated



**Table 3** Resistivity and conductivity of as-deposited and annealed TiO<sub>2</sub> thin films

Annealing temperature (°C)	Resistivity, $\rho$ ( $\Omega$ cm)	Conductivity, $\sigma$ (siemens/m)
As-deposited	2.5751E+8	3.883E−9
300	1.6695E+8	5.990E−9
500	1.5869E+8	6.302E−9
700	7.768E+7	1.287E−8
900	6.714E+7	1.489E−8

electron–hole pairs (Hanini et al. 2013; Zhao et al. 2008). As a result, Ti<sup>4+</sup> ion have greater concentration in the films which annealed at higher annealing temperature, which eventually caused an increase in the free electrons concentrations and subsequently caused reduction in films resistivity. The values of the calculated resistivity and conductivity are tabulated in Table 3.

It is well known that the electrical conductivity of TiO<sub>2</sub> is affected by oxygen vacancies which are intrinsic for any oxide material and act as electron donors that can influence the n-type TiO<sub>2</sub> conductivity (Pomoni et al. 2011). In Table 3, the electrical conductivity increased as following this order: as-deposited <300 °C <500 °C <700 °C <900 °C, indicates that the resistivity of the annealed TiO<sub>2</sub> thin films decreased with increasing annealing temperatures. It can be explained that at a higher annealing temperatures, the band gap between the valence and conduction bands became smaller and consequently, smaller energy was used for electrons to be excited from the occupied band (valence band) to the unoccupied band (conduction band) (Sarah et al. 2010). Thus, more electrons were jump to the conduction band and consequently, the conductivity was increased. The electrical conductivity can be described in the following equation:

$$\text{Conductivity, } \sigma = \frac{1}{\rho} \quad (7)$$

where  $\sigma$  is the conductivity inverse proportional to the resistivity,  $\rho$ . The conductivity and resistivity data that shown in Table 3 are in agreement with that Eq. 7. Owing to the lowest conductivity and highest resistivity of as-deposited thin film, it is reasonable to speculate that more energy was needed to excite electrons from valence band to conduction band. Therefore, smaller amount of electrons flowed in the conduction band and decreased the conductivity of as-deposited thin films.

## 4 Conclusion

The effects of different annealing temperatures on the morphology, optical and electrical properties of TiO<sub>2</sub> films

were studied. The XRD results suggest that the presence of amorphous, tetragonal anatase and mixed anatase/rutile phase structures were affected by increasing annealing temperatures. The surface roughness increased with increasing annealing temperatures. UV–vis results show that the optical band gap energy of TiO<sub>2</sub> thin films decreased with increasing annealing temperatures in the range of 3.79–3.16 eV (direct allowed) and 3.95–3.75 eV (indirect allowed) which closely related to an increases of the grain sizes of TiO<sub>2</sub> thin films. It was further found that the TiO<sub>2</sub> thin films became translucent after annealed at higher temperatures and subsequently, reduced the transmittance. This is basically due to the annihilation of porous surfaces which caused by the particles sizes growth, phase transformation from nanocrystalline anatase to rutile phase and the light scattering in the films. Lastly, as the annealing temperatures increased, the resistivity of the TiO<sub>2</sub> thin films decreased and lead to the higher electrical conductivity of TiO<sub>2</sub> thin films. In short, our present work highlights the key significance of rational engineering of TiO<sub>2</sub> thin films by coupling with SiO<sub>2</sub>/p-Si as the next generation MIS structure, which would bring huge potential to remarkably improve the dielectric constant and higher breakdown strength of SiO<sub>2</sub>/p-Si for addressing the current and future semiconductor-related issues.

**Acknowledgments** This research is supported by University of Malaya Research Grant (UMRG: CG003-2013). The authors would like to express their deepest appreciation especially to Prof. Dr. Uda bin Hashim for his guidance and knowledge shared in the completion of this research and to all members Institute of Nano Electronic Engineering (INEE) and School of Microelectronic Engineering (SoME), UniMAP. The authors would also like to thank Mr Hasrul and Mrs Mira for providing the technical assistance.

**Conflict of interest** The authors confirm that this article does not have content with conflict of interest.

## References

- Addamo M, Augugliaro V, Paola AD, Lopez EG, Loddo V, Marci G, Molinari R et al (2004) Preparation, characterization, and photoactivity of polycrystalline nanostructured TiO<sub>2</sub> catalysts. *J Phys Chem B* 108(10):3303–3310
- Ahmad MK, Halid MLM, Rasheid NA, Ahmed AZ, Abdullah S, Rusop M (2010) Effect of annealing temperatures on surface morphology and electrical properties of titanium dioxide thin films prepared by sol gel method. *J Sustain Energy Environ* 1:17–20
- Al-Obaidi SS, Yousif AA (2013) Synthesis of nanostructured TiO<sub>2</sub> thin films by pulsed laser deposition (PLD) and the effect of annealing temperature on structural and morphological properties. *Ibn Al-Haitham Jour for Pure Appl Sci* 26(3):143–152
- Brinker CJ, Harrington MS (1981) Sol-gel derived antireflective coatings for silicon. *Sol Energ Mater* 5(2):159–172
- Campbell SA, Gilmer DC, Xiao-Chuan W, Ming-Ta H et al (1997) MOSFET transistors fabricated with high permittivity TiO<sub>2</sub> dielectrics. *IEEE T Electron Dev* 44:104–109

- Choi HW, Jin YS, Kim KH (2010) Properties of TiO<sub>2</sub> films prepared for use in dye-sensitized solar cells by using the sol-gel method at different catalyst concentrations. *J Korean Phys Soc* 57(4):1049–1053
- Çörekçi S, Kizilkaya K, Asar T, Öztürk MK, Özçelîk S (2011) Effects of thermal annealing and film thickness on the structural and morphological properties of titanium dioxide films. *Proc Int Congr Adv Appl Phys Mater Sci* 121(1):247–248
- De Anda Reyes ME, Torres Delgado G, Castanedo Pérez R, Márquez Marián J et al (2012) How room-humidity during the coating affects the structural, optical and photocatalytic properties of TiO<sub>2</sub> films. *J Sol-Gel Sci Techn* 61:310–315
- Dubal DP, Dhawale DS, More AM, Lokhande CD (2011) Synthesis and characterization of photosensitive TiO<sub>2</sub> nanorods by controlled precipitation route. *J Mater Sci* 46(7):2288–2293
- Enache-Pommer E, Boercker JE, Aydil ES (2007) Electron transport and recombination in polycrystalline TiO<sub>2</sub> nanowire dye-sensitized solar cells. *Appl Phys Lett* 91:123116
- Foo KL, Kashif M, Hashim U (2011) Study of ZnO thin film on silicon substrate by sol-gel spin coating method for bio-medical application. In: International conference on biomedical engineering (ICoBE) 27–28 February 2012, pp 223–226
- Foo KL, Kashif M, Hashim U (2012a) Study of zinc oxide films on SiO<sub>2</sub>/Si substrate by sol-gel spin coating method for pH measurement. *Appl Mech Mater* 284:347–351
- Foo KL, Kashif M, Hashim U, Ali ME (2012b) Sol-gel derived ZnO nanoparticulate films for ultraviolet photodetector (UV) applications. *Optik* 124(22):5373–5376
- Foo KL, Hashim U, Prasad H, Kashif M (2012c) Fabrication and characterization of IDE ZnO thin films using sol-gel method for PBS solution measurement. In: International conference on semiconductor electronics. 19–21 September 2012, pp 736–739
- Foo KL, Kashif M, Hashim U, Ali ME (2013) Fabrication and characterization of ZnO thin Films by sol-gel spin coating method for the determination of phosphate buffer saline concentration. *Curr Nanosc* 9(2):288–292
- Foo KL, Kashif M, Hashim U, Wei-Wen L (2014) Effect of different solvents on the structural and optical properties of zinc oxide thin films for optoelectronic applications. *Ceram Int* 40(1):753–761
- Gou X, Ma TP (1998) Tunneling leakage current in oxynitride: dependence on oxygen/nitrogen content. *IEEE Electr Device L* 19:207–209
- Gugliemi M, Colombo P, Mabcielli Degli Esposti L (1992) Characterization of laser-densified sol-gel films for the fabrication of planar and strip optical waveguides. *J Non-Cryst Solids* 147–148:641–645
- Habibi MH, Nasr-Esfahani M, Emtiazi G, Hosseinkhani B (2010) Nanostructure thin films of titanium dioxide coated on glass and its anti UV effect for living organisms. *Current Nanosci* 6(3):324–329
- Hanini F, Bouabellou A, Bouachiba Y, Kermiche F, Taabouche A et al (2013) Structural, optical and electrical properties of TiO<sub>2</sub> thin films synthesized by sol-gel technique. *IOSR J Eng* 3(11):21–28
- Hasan MM, Haseeb ASMA, Saidur R, Masjuki HH (2008) Effect of annealing treatment on optical properties of Anatase TiO<sub>2</sub> thin films. *World Acad Sci Eng Technol* 16:221–225
- Horprathum M, Eiamchai P, Chindaudom P, Pokaipisit A, Limsuwan P (2012) Oxygen partial pressure dependence of the properties of TiO<sub>2</sub> thin films deposited by DC reactive magnetron sputtering. In: *Procedia Engineering* 32:676–682
- Hosseini A, Icli KC, Gullu HH (2013) Preparation and characterization of porous TiO<sub>2</sub> thin films by sol-gel method for extremely thin absorber-ETA solar cell applications. *Turk J Sci Technol* 8(2):69–79
- Janitabar-Darzi S, Mahjoub AR, Nilchi A (2009) Investigation of structural, optical and photocatalytic properties of mesoporous TiO<sub>2</sub> thin film synthesized by sol-gel templating technique. *Physica E* 42(2):176–181
- Jin Kim D, Hong Hahn S, Hoon OhS, Jung Kim E (2002) Influence of calcination temperature on structural and optical properties of TiO<sub>2</sub> thin films prepared by sol-gel dip coating. *Mater Lett* 57(2):355–360
- Jing-Xiao L, Da-Zhi Y, Shi F, Ying-Ji C (2003) Sol-gel deposited TiO<sub>2</sub> film on NiTi surgical alloy for biocompatibility improvement. *Thin Solid Films* 429:225–230
- Justicia I, Ordejon P, Canto G, Mozos JL, Fraxedas J, Battiston GA et al (2002) Designed self-doped titanium oxide thin films for efficient visible-light photocatalysis. *Adv Mater* 14(19):1399–1402
- Kabasakaloğlu M, Talu M, Yıldırım F, Sarı B (2003) The electrochemical homopolymerization of furan and thiophene and the structural elucidation of their bipolymer films. *Appl Surf Sci* 218(14):85–97
- Kumar S, Verma NK, Singla ML (2012) Sized dependent reflective properties of TiO<sub>2</sub> nanoparticles and reflectors made thereof. *Dig J Nanomater Bios* 7(2):607–619
- Li-jian M, Andritschky M, Dos Santos MP (1993) The effect of substrate temperature on the properties of d.c. reactive magnetron sputtered titanium oxide films. *Thin Solid Films* 223:242–247
- Lottiaux M, Boulesteix C, Nihoul G, Varnier F, Flory F, Galindo R, Pelletier (1989) Morphology and structure of TiO<sub>2</sub> thin layers vs. thickness and substrate temperature. *Thin Solid Films* 170(1):107–126
- Mathews NR, Corte Jacome MA, Morales ER, Toledo Antonio JA (2009a) Structural and spectroscopic study of the Fe doped TiO<sub>2</sub> thin films for applications in photocatalysis. *Phys Status Solidi (c)* 6:219–223
- Mathews NR, Morales ER, Cortes-Jacome MA, Toledo Antonio JA (2009b) TiO<sub>2</sub> thin films- Influence of annealing temperature on structural, optical and photocatalytic properties. *Sol Energy* 83:1499–1508
- Mayabadi AH, Waman VS, Kamble MM, Ghosh SS, Gabhale BB et al (2014) Evolution of structural and optical properties of rutile TiO<sub>2</sub> thin films synthesized at room temperature by chemical bath deposition method. *J Phys Chem Solids* 75(2):182–187
- Mulayam S, Varshney GR, Bhaduria S (2010) Biogenic synthesis of silver nanocubes and nanorods using sundried Stevia rebaudiana leaves. *Adv Mat Lett* 1(3):232–237
- Ohno T, Sarukawa K, Matsumura M (2001) Photocatalytic activities of pure rutile particles isolated from TiO<sub>2</sub> powder by dissolving the anatase component in HF solution. *J Phys Chem B* 105(12):2417–2420
- Ohno T, Tokieda K, Higashida S, Matsumura M (2003) Synergism between rutile and anatase TiO<sub>2</sub> particles in photocatalytic oxidation of naphthalene. *Appl Catal A* 244(2):383–391
- Oja I, Mere A, Krunks M, Nisumaa R, Solterbeck C-H, Es-Souni M (2006) Structural and electrical characterization of TiO<sub>2</sub> films grown by spray pyrolysis. *Thin Solid Films* 515(2):674–677
- Paily R, DasGupta A, DasGupta N, Bhattacharya P, Misra P, Ganguli T et al (2002) Pulsed laser deposition of TiO<sub>2</sub> for MOS gate dielectric. *Appl Surf Sci* 187:297–304
- Paul R, Jr Ohodnicki, Wang CJ, Natesakhawat S, John PB, Thomas DB (2012) In-situ and ex situ characterization of TiO<sub>2</sub> and Au nanoparticles incorporated TiO<sub>2</sub> thin films for optical gas sensing at extreme temperatures. *J Appl Phys* 111(6):064320
- Pomoni K, Vomvas A, Todorova N, Giannakoulou T, Mergia K, Trapalis C (2011) Thermal treatment effect on structure, electrical conductivity and transient photoconductivity behavior of thiourea modified TiO<sub>2</sub> sol-gel thin films. *J Alloy Compd* 509(26):7253–7258
- Richards BS (2002) Novel uses of titanium dioxide for silicon solar cells. Ph.D. thesis, University of New South Wales, Sydney, Australia

- Sarah MSP, Musa MZ, Asiah MN, Rusop M (2010) Electrical Conductivity Characteristics of TiO<sub>2</sub> Thin Film. In: International conference on electronic devices, systems and applications (ICEDSA). 11–14 April 2010, pp 361–364
- Spurr RA, Myers H (1957) Quantitative analysis of anatase-rutile mixtures with an X-ray diffractometer. *Anal Chem* 29(5):760–762
- Subramaniam S, Chitra lekha P, Padiyan PD (2009) Inclusion of polyaniline in electrodeposited bismuth sulphide thin films: synthesis and characterization. *Curr Appl Phys* 9(5):1140–1145
- Tachibana Y, Akiyama HY, Kuwabata S (2007) Optical simulation of transmittance into a nanocrystalline anatase TiO<sub>2</sub> film for solar applications. *Sol Energ Mat Sol C* 91:201–206
- Tauc J, Grigorovici R, Vancu A (1966) Optical properties and electronic structure of amorphous germanium. *Phys Status Solidi* 15(2):627–637
- Tayade RJ, Surolia PK, Kulkarni RG, Jasra RV (2007) Photocatalytic degradation of dyes and organic contaminants in water using nanocrystalline anatase and rutile TiO<sub>2</sub>. *Sci Technol Adv Mater* 8(6):455–462
- Turkevych I, Pihosh Y, Goto M, Kasahara A, Tosa M, Kato S, Takehana K et al (2008) Photocatalytic properties of titanium dioxide sputtered on a nanostructured substrate. In: The 7th international conference on nano-molecular electronics thin solid films 516(9):2387–2391
- Wei G, Zhang Y, Xiong R (2003) Controllable preparation of nano-sized TiO<sub>2</sub> thin film and relationship between structure of film and its photocatalytic activity. *Sci China Ser B* 46(2):184–190
- Ya-Qi H, Da-Ming Z, Zhao G, Min-Sheng W (2003) Influence of annealing temperature on the properties of titanium oxide thin film. *Appl Surf Sci* 218(1–4):98–106
- Yaşa I, Lkhagvajav N, Koizhaiganova M, Çelik E, Sarı O (2012) Assessment of antimicrobial activity of nanosized Ag doped TiO<sub>2</sub> colloids. *World J Microb Biot* 28:2531–2539
- Zachariah A, Baiju KV, Shukla S, Deepa KS, James J et al (2008) Synergistic effect in photocatalysis as observed for mixed-phase nanocrystalline titania processed via sol-gel solvent mixing and calcination. *J Phys Chem C* 112(30):11345–11356
- Zhao X, Zhao Q, Yu J, Liu B (2008) Development of multifunctional photoactive self-cleaning glasses. *J Non-Cryst Solids* 354(12–13):1424–1430
- Zhu J, Yang J, Zhen-Fen B, Ren J, Yong-Mei L, Cao Y, He-Xing et al (2007) Nanocrystalline anatase TiO<sub>2</sub> photocatalysts prepared via a facile low temperature nonhydrolytic sol-gel reaction of TiCl<sub>4</sub> and benzyl alcohol. *Appl Catal B-Environ* 76(1–2):82–91